Available online at www.sciencedirect.com

ScienceDirect

Ceramics International 40 (2014) 1651–1660

CERAMICS INTERNATIONAL

www.elsevier.com/locate/ceramint

Effect of calcination temperature for magnesite on interaction of MgO-rich phases with boric acid

Keiko Sasaki[a,*], Sayo Moriyama[b]

[a]Department of Earth Resource Engineering, Kyushu University, Fukuoka 819-0395, Japan
[b]Fukuoka Prefecture Institute of Health and Environmental Sciences, Fukuoka 818-0135, Japan

Received 29 June 2013; received in revised form 11 July 2013; accepted 11 July 2013
Available online 19 July 2013

Abstract

Magnesia (MgO), which can be obtained by calcination of natural magnesite, is one of the most effective known sorbents for borate in aqueous solutions. Here we examine the effect of calcination temperature on sorption of borate for MgO-rich phases produced by calcination of magnesite at 873–1373 K. Calcination at or above 1273 K produced a single magnesium oxide phase, whereas basic magnesium carbonates ($m\mathrm{MgCO_3} \cdot n\mathrm{Mg(OH)_2} \cdot x\mathrm{H_2O}$) formed in association with magnesium oxide at or below 1073 K. Calcination temperature directly affected the efficiency of decarbonation of magnesium carbonate, and the solubility and basicity of magnesium oxide in the resultant calcined products. These factors (along with the boron concentration) essentially control the immobilization mechanism of borate on the calcined MgO-rich phases. After sorption of borate on products calcined at lower temperatures, different types of basic magnesium carbonates were formed that are less effective at immobilizing borate. At low borate concentrations, under saturation for magnesium borate hydrate ($Mg_7B_4O_{13} \cdot 7H_2O$), co-precipitation of borate with $Mg(OH)_2$ predominates. However, as magnesium borate hydrate becomes supersaturated, both precipitation of $Mg_7B_4O_{13} \cdot 7H_2O$ and co-precipitation with $Mg(OH)_2$ contribute significantly to borate immobilization. Calcination temperature is a key practical factor affecting the borate sorption efficiency by changing the immobilization mechanism.

Keywords: Borate; Calcination temperature; Magnesium oxide; Magnesium borate hydrate; Basicity

1. Introduction

Boron is known to be an essential element for living plants, animals and humans [1]. However, excess intake of boron sometimes causes problems such as nervous system disorders [2] and infertility [3]. Because of its potential toxicity, the maximum contaminant levels of boron are regulated by the World Health Organization at 10 mg L^{-1} for industrial discharges and 1 mg L^{-1} for drinking water [4]. Boron is sometimes discharged from mining sites, and from electronic, semi-conductor and glass factories, potentially resulting in groundwater contamination [5]. Permeable reactive barriers (PRBs) are used in in situ groundwater remediation for the removal of contaminants [6–8]. However, PRBs have not been applied in practice to remove boron from groundwater, because cost-effective reactive materials are yet to be found. Advanced materials, like boron-selective resins and membranes, have been intensively developed [9], but are unsuitable for PRBs. Materials in PRBs must have appropriate reactivity, permeability, availability and cost. Until now, immobilization of borate on inorganic materials such as activated carbon [10], activated alumina [11], clay minerals [12–14] and fly ash, [15] has been investigated. In these approaches, low capacities and inconsistent quality are some of the drawbacks. Of the materials tested, the highest reactivity was observed with magnesium oxide [16,17].

Magnesium oxide is a common material, which can be obtained by calcination of the natural minerals, magnesite (Mg_2CO_3) and/or hydromagnesite ($Mg_2(CO_3)(OH)_2$) [18]. Magnesium oxide has been used for immobilization of not only anionic species but also heavy metals [19,20]. In these reactions, the immobilization mechanism is mainly based on co-precipitation with $Mg(OH)_2$. In other words, calcined MgO-rich phases are destroyed during the immobilization and transformed into hydroxides. The calcination conditions

*Corresponding author. Tel./fax: +81 92 802 3338.
E-mail address: keikos@mine.kyushu-u.ac.jp (K. Sasaki).

0272-8842/$ - see front matter
http://dx.doi.org/10.1016/j.ceramint.2013.07.056

affect the reactivity in applications. For example, Birchal et al. have reported that the higher calcination temperature of magnesite showed higher conversion levels of hydration [21]. This suggests the basicity of magnesium oxide is influenced by the calcination temperature. The immobilization mechanism of borate with magnesium oxide involves ligand-promoted dissolution of magnesium oxide [22]. While chelating reagents inhibit MgO hydration [23], borate is a weak ligand so hydration happens in the presence of borate. Additionally, precipitates which form and include the target species need to be considered, because precipitation is also a very effective sink for target species. In the present work, the effect of the calcination temperature used to produce magnesium oxide from magnesite on the removal of borate is discussed, and is related to the borate removal mechanism.

2. Experimental

MgO-rich phases were produced by heating magnesium carbonate (special grade, Sigma-Aldrich, St. Louis, MO, US) using an electric furnace TME 2200 (EYELA, Tokyo, Japan) from room temperature to the reaction temperature (873, 1073, 1273 or 1373 K) at 15 °C/min, holding at temperature for 1 h under static air, and then cooling down naturally to room temperature. The calcined products were stored in a low humidity storage case V-30 (Shinei, Osaka, Japan) prior to use, and characterization and borate sorption experiments were performed within a week. Under these conditions, decarbonation of magnesium carbonate primarily produces magnesium oxide. Thus the products are termed: MgO873, MgO1073, MgO1273, and MgO1373, respectively.

The products calcined at different temperatures were characterized by X-ray diffraction (XRD, Multi Flex, Rigaku, Akishima, Japan) using Cu Kα radiation at 20 mA and 40 kV for crystal phase identification and evaluation of lattice strain (η) and crystal size (ε). The η and ε values for each calcined product were calculated by the Halder–Wagner method [24], as shown in

$$\frac{\beta^*}{d^*} = \left(\frac{1}{\varepsilon}\right)\left(\frac{\beta}{d^*}\right)^2 + \frac{\eta^2}{2}, \tag{1}$$

where β is the peak width at half height of a diffraction peak (corrected for instrument broadening using a Si standard), d^* is $2\sin\theta/\lambda$ and β^* is $\beta\cos\theta/\lambda$. The values of η and ε can be obtained from plots of β^*/d^* versus $(\beta/d^*)^2$ [25].

Measurements of specific surface areas were performed using a gas sorption analyzer (Autosorb-1, Yuasa, Osaka, Japan) and the seven-point Brunauer–Emmett–Teller (BET) method. The average specific gravity of each calcined product was determined using an Ostwald type pycnometer.

Temperature programmed desorption curves for carbon dioxide (CO_2-TPD) were also acquired to evaluate basicity and the numbers of basic sites of the calcined products. The measurements were performed using a gas absorption measurement instrument BEL SORP (Bel Japan Inc., Toyonaka, Japan), with carbon dioxide as a probe gas. After pre-treatment by heating at 973 K for 50 min, CO_2-TPD curves were measured from room temperature to 1023 K. Peak deconvolutions were performed using a Chem Master ver. 1.2.0.2 (Bel Japan Inc.).

Scanning electron microscopic (SEM) images were obtained using a VE-9800 SEM (KEYENCE, Osaka, Japan) with a 15 kV acceleration voltage; transmission electron microscopic (TEM) images were obtained with an FEI TECNAI-20 (JEOL, Tokyo, Japan) TEM.

Borate sorption experiments were carried out with an initial H_3BO_3 (Wako, special grade) concentration of 6.08 mM at pH 9.0 ± 0.1, as adjusted with 0.2 M sodium hydroxide. 0.12 g of calcined product was added to 40 mL of the above borate solution in a plastic bottle. Each bottle was tightly sealed with a plastic cap, laid down and horizontally shaken on a rotary shaker (Takasaki Kagaku, Co. ltd, Kawaguchi, Japan) at 100 rpm and 298 K until equilibrium was achieved. At intervals, 1.0 mL of supernatant was sampled from each bottle, and filtered; the concentrations of boron and magnesium ions within the solution were evaluated by inductively coupled plasma atomic emission spectrometry (ICP-AES, VISTA-MPX, Seiko Instruments, Chiba, Japan). To obtain sorption isotherms of borate on the calcined, MgO-rich phase products, additional batch tests were conducted using 0.10 g of sorbents in 1.00–67.90 mM borate solutions at an initial pH of 9.0 ± 0.1.

Solid residues after borate sorption equilibrium tests were collected and freeze-dried. XRD, SEM and TEM measurements were carried out as mentioned previously, and the boron to magnesium molar ratio was calculated by determination of residual dissolved concentrations using ICP-AES.

3. Results and discussion

Fig. 1 shows the XRD patterns for the products calcined at 873–1373 K. The XRD patterns for products calcined at 1273 K or more showed the formation of a well crystallized, single phase of magnesium oxide (JCDPS 45-946). With decrease in calcination temperature, less crystalline magnesium oxide was formed. After calcination at 1073 K, small amounts of $Mg_2CO_3(OH)_2 \cdot 0.5H_2O$ were found (JCPDS 37-454), along with less crystalline magnesium oxide as the predominant phase. At 873 K, uncalcined magnesium carbonate ($MgCO_3 \cdot 5H_2O$, JCPDS 35-680) also remained, as well as less crystalline magnesium oxide and $Mg_2CO_3(OH)_2 \cdot 0.5H_2O$. Thus, decarbonation of magnesium carbonate is incomplete after calcination at temperatures of 1073 K or less [26].

The Halder–Wagner [24] plots based on the results in Fig. 1 are depicted in Fig. 2. The correlation coefficient was more than 0.95 in all cases. The slope was much steeper for MgO873 than for the other samples (Fig. 2(a)), so the plots for MgO1073, MgO1273 and MgO1373 were presented with expanded y-axes in Fig. 2(b). Higher calcination temperatures were found to produce larger crystal sizes (ε) and smaller lattice strains (η); calcination temperatures above 873 K significantly changed the structural characteristics of the magnesium oxide. The ε and η values for the magnesium oxide phase are summarized in Table 1.

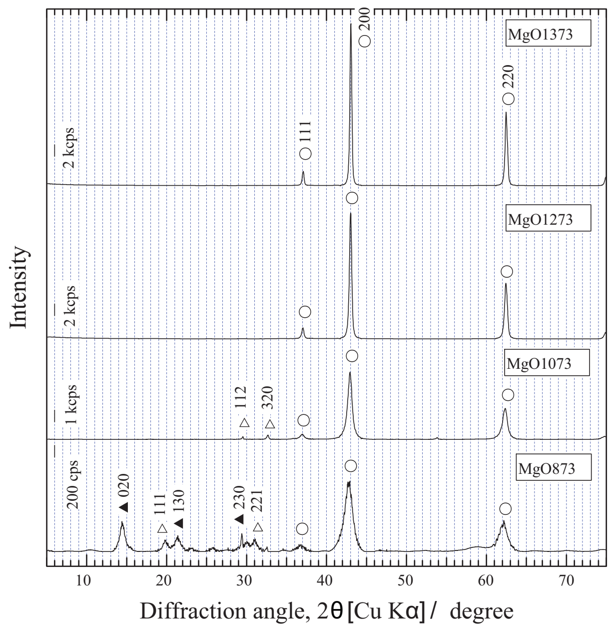

Fig. 1. XRD patterns of products after calcination of $MgCO_3$ for 1 h at 873, 1073, 1273, or 1373 K. Symbols: ○, MgO (JCPDS 45-946); △, $Mg_2CO_3(OH)_2 \cdot 0.5H_2O$ (JCPDS 37-454); ▲, $MgCO_3 \cdot 5H_2O$ (JCPDS 35-680).

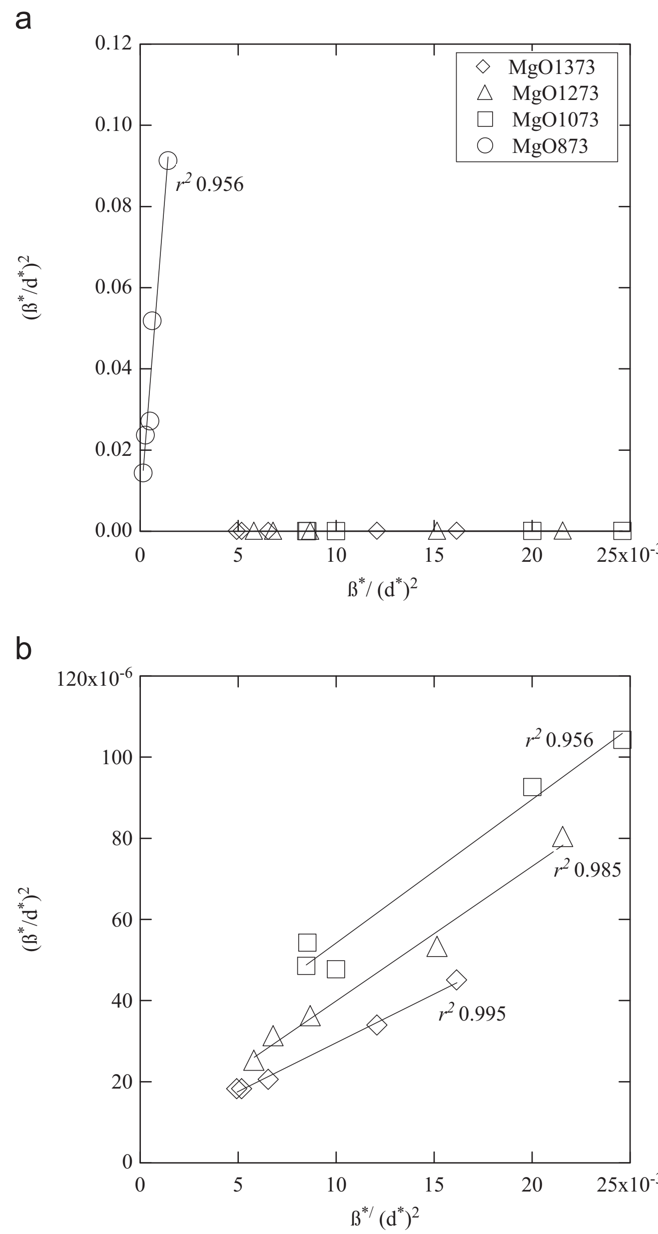

Fig. 2. Estimation of crystal size (ε) and lattice strain (η) by Halder–Wagner plots for MgO873, MgO1073, MgO1273, and MgO1373. Correlation coefficients are 0.956, 0.956, 0.985 and 0.995 for MgO873, MgO1073, MgO1273, and MgO1373, respectively.

Fig. 3 shows TEM images of the calcined products, again indicating increase in crystal size with increase in calcination temperature. Aggregation of hexagonal and rectangular plates was more clearly observed at higher calcination temperatures. Compared with the crystal sizes estimated from powder XRD (Table 1), direct observation showed much smaller sizes (10–60 nm). This difference has sometimes been observed with other powders, because of size distribution [27]. The electron diffraction patterns also confirmed that higher crystallinity was obtained at higher calcination temperature.

As shown in Table 1, the specific surface areas of the calcined products decreased with increase in calcination temperature above 1073 K. The average specific gravity of the calcined product was 2.29 g/cm^3 for MgO873, and increased with increasing calcination temperature to approach 3.58 g/cm^3, the theoretical value for MgO [28], for MgO1373. The products calcined at lower temperatures are characterized by imperfect decarbonation, and magnesium carbonates have lower densities [29], e.g. 1.85 g/cm^3 for $MgCO_3 \cdot 3H_2O$. Changes in specific surface area reflected both decarbonation and sintering. The decarbonation process results in an increase in specific surface area, but the additional sintering process, which occurs more in the samples sintered at 1073–1273 K, decreases the specific surface area. Both decarbonation and sintering are enhanced with increasing calcination temperature.

The CO_2-TPD curves were collected, converted into sorbed mass of carbon dioxide per unit surface area, and deconvoluted into three components, as shown in Fig. 4. The sorbed mass of carbon dioxide per specific surface area decreased with decrease in calcination temperature. The basicity around 370 °C has been previously shown to increase with increasing calcination temperature, which affects hydration [21,23].

Fig. 5 shows examples of batch sorption, to demonstrate the effect of calcination temperature on changes in boron and magnesium concentrations in solutions and on pH, for an initial boron concentration of 6.08 mM. The equilibrium boron concentrations were in the order: MgO1373 ∼ MgO1273 < MgO1073 < MgO873 (Fig. 5(a)). This is clearly related to the fact that there is less magnesium oxide in MgO873 than in the other sorbents (as shown in Fig. 1). Soon after contact of magnesium oxide with boric acid, magnesium ions were released (Fig. 5(b)). As reported in the previous work [17], the larger amounts of magnesium ions released from MgO873 were derived from the less crystalline magnesium oxide within this sorbent, not from carbonates, because the carbonates are

Table 1
BET specific surface area, specific gravity, crystal size (ε) and lattice strain (η) for calcined products at different temperatures. ε and η were estimated by Halder–Wagner plots in Fig. 2.

	BET specific surface area (m^2/g)	Specific gravity (g/cm^3)	Crystal size, ε (nm)	Lattice strain, η
MgO 873	49.8	2.29	61	0.0063
MgO1073	79.0	3.14	275	0.0056
MgO1273	29.1	3.44	298	0.0022
MgO1373	12.7	3.58	414	0.0026

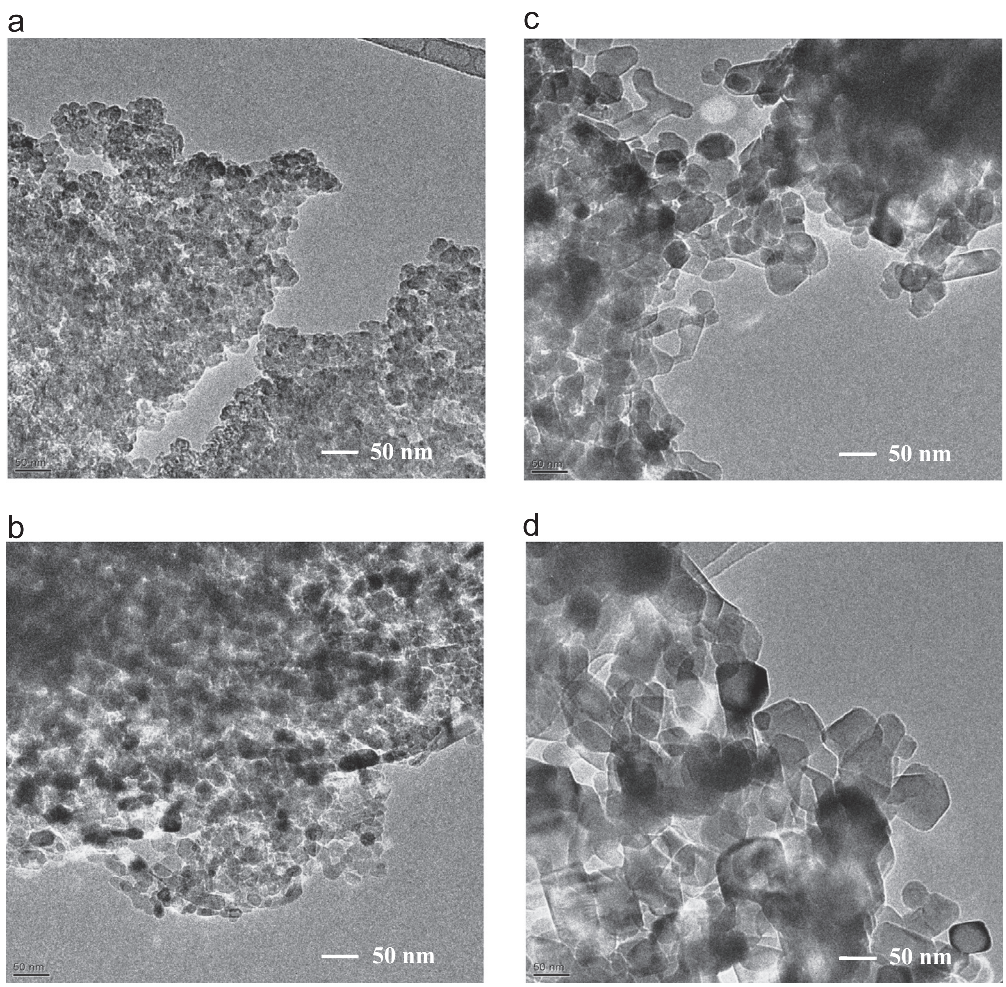

Fig. 3. TEM images of (a) MgO873, (b) MgO1073, (c) MgO1273, and (d) MgO1373.

less soluble than magnesium oxide. However, the quantity of magnesium ions released from MgO873 cannot be explained by the solubility only, because the concentration is approximately twice that of a "background" sample (i.e., when the sorbent was immersed in water rather than boron-containing solution).

This suggests that some additional mechanism exists. Also, more than 1 mM of magnesium ions was initially released from the other calcined products. This phenomenon has not been observed during sorption of fluoride on these calcined products [17], and is considered to be derived from reaction mechanisms of magnesium oxide with borate that differ from those with fluoride. Both immobilizations are based on co-precipitation with $Mg(OH)_2$, which is a hydration product of MgO. During reaction of magnesium oxide with boric acid, Mg^{2+} ions are complexed with H_3BO_3 to form $[MgB(OH)_4]^+$ ($K = 10^{-1.34}$–$10^{-1.63}$ at 25 °C, [30]), leading to ligand-promoted dissolution of magnesium oxide. Separately, it has been observed that larger initial boron concentrations induced release of greater amounts of magnesium ions from the same magnesium oxide sorbents [22]. Ligand-promoted dissolution of magnesium oxide is not observed with fluoride.

The equilibrium pH was clearly higher for samples calcined at higher temperatures (Fig. 5(**c**)); this would facilitate the precipitation of $Mg(OH)_2$, resulting in lower equilibrium magnesium ion concentrations (Fig. 5(b)). It has been

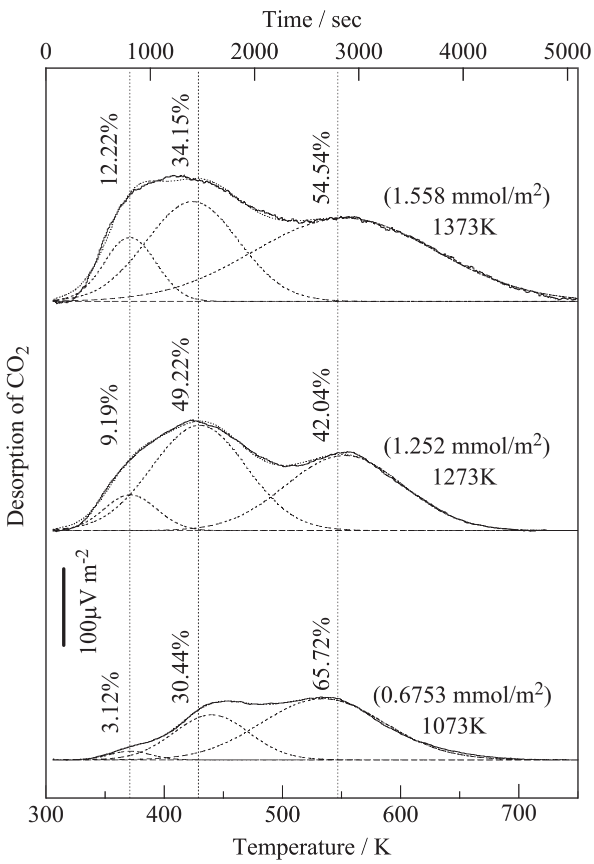

Fig. 4. CO_2-TPD curves and their deconvolution for products calcined at different temperatures. The numbers in brackets indicate total basicities expressed as mass of carbon dioxide sorbed per unit surface area. Percentages indicate the relative areas of each peak after deconvolution.

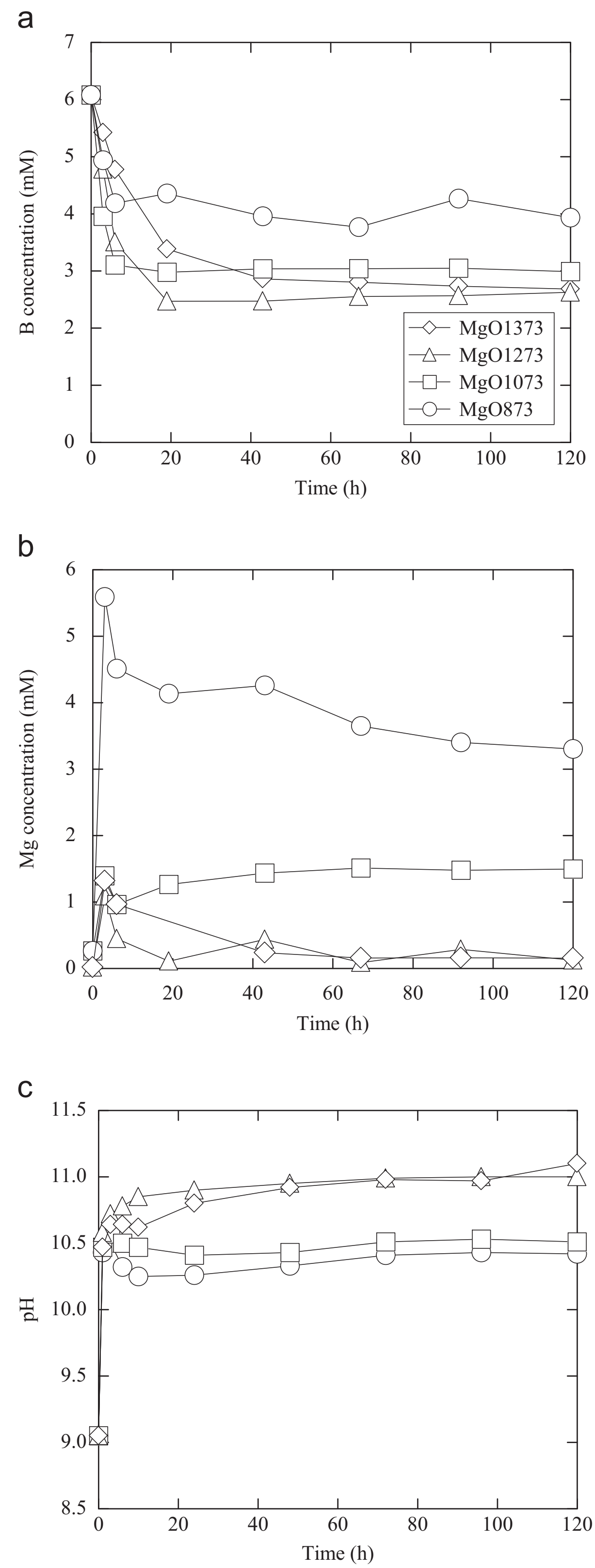

Fig. 5. Changes of (a) boron concentration, (b) magnesium concentration, and (c) pH with time during sorption of 6.08 mM boron at 298 K on 0.12 g of products calcined at different temperatures.

suggested that there is a competition between water and H_3BO_3 to access the surfaces of magnesium oxide [31]. The rate of sorption of borate was highest for MgO1073, followed by MgO1273 and MgO1373 (Fig. 5(a)). This was probably because of faster hydration of the higher temperature-calcined products (which have greater basicities); this hydration then interferes with access of H_3BO_3 to MgO surfaces.

The effects of calcination temperature on the sorption isotherms of borate on calcined products are depicted in Fig. 6. The numbers on the figure indicate the initial boron concentrations in mM. There is a trend that greater sorption densities were obtained with products calcined at higher temperatures, although the sorption density of borate is very similar for MgO1273 and MgO1373 at all the equilibrium concentration (C_e) values studied (Fig. 6(a)). When C_e is less than 2 mM (Fig. 6(b)), the performance of MgO1073 is also similar to that of the samples calcined at higher temperatures. MgO873 includes non-negligible amounts of $Mg_2CO_3(OH)_2$ and $MgCO_3$, which do not meaningfully contribute to sorption of borate [23], as shown in Fig. 1. Sorption isotherms of borate increased sharply at $C_e \geqq 30$ mM, indicating that there are additional sorption mechanisms which depend on the concentration of borate.

The sorption density of borate is not obviously influenced by the specific surface areas of the calcined products, because of destructive sorption [23], but by the basicity per unit surface area (Fig. 4). This trend was also observed for the sorption of fluoride, that is, a larger basicity per unit surface area was

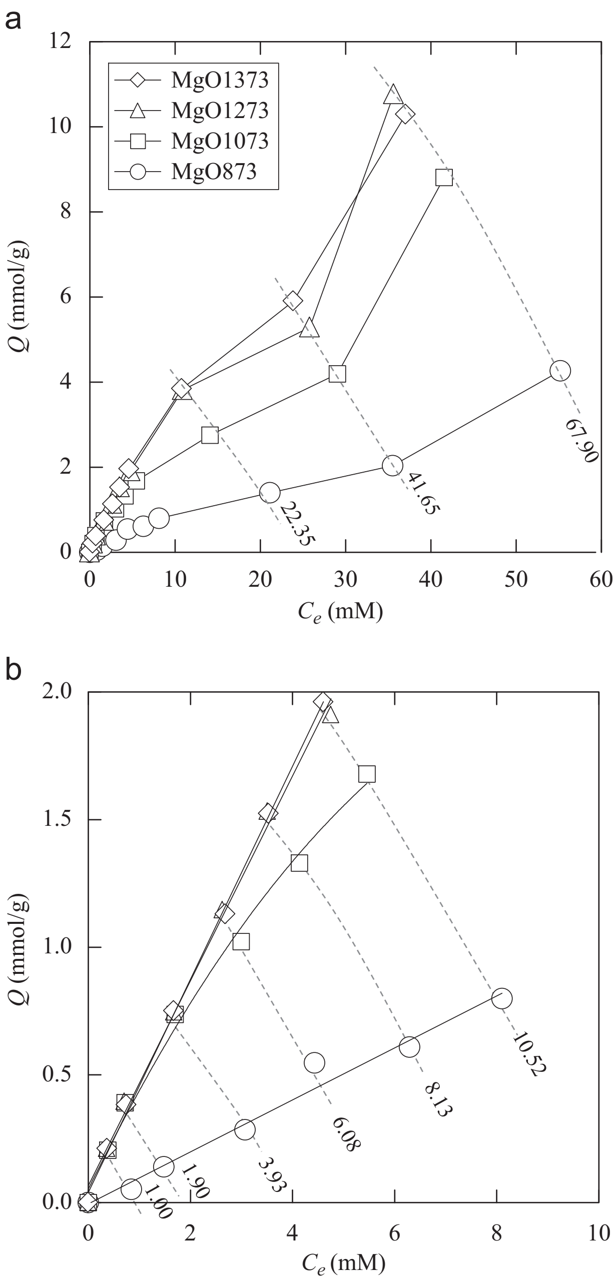

Fig. 6. Sorption isotherms of boron on magnesium oxide calcined at different temperatures. The region of $C_e < 10$ mM in (a) is expanded in (b). The numbers (mM) in both figures indicate the initial boron concentrations.

observed at higher calcination temperature [17]. However, there is a difference between the effects of calcination temperature on sorption densities of fluoride and borate. Products calcined at lower temperatures tended to show larger sorption densities of fluoride at higher C_e of fluoride, as a result of the formation of $Mg(OH)_{2-x}F_x$ [17]. In the case of fluoride, sorption isotherms could be fitted to Freundlich-type isotherm equations, without any regions where the gradient of the curve increased. However, for sorption isotherms of borate, products calcined at higher temperatures consistently showed larger sorption densities, independent of borate concentrations; regions of increasing gradient were also seen at $C_e \geqq 30$ mM (Fig. 6(a)).

XRD patterns for solid residues from MgO-rich phases calcined at 873–1373 K, after sorption equilibrium tests in 6.08 mM and 67.9 mM borate solutions, are shown in Fig. 7 (a) and (b). The solid residues include brucite ($Mg(OH)_2$, JCPDS 44 = 1482) as the dominant phase in most cases. At an initial concentration of 6.08 mM, poorly crystallized hydromagnesite ($Mg_5(CO_3)_4(OH)_2 \cdot 4H_2O$, JCPDS 25-513) was also formed, along with $Mg(OH)_2$, for all calcination temperatures.

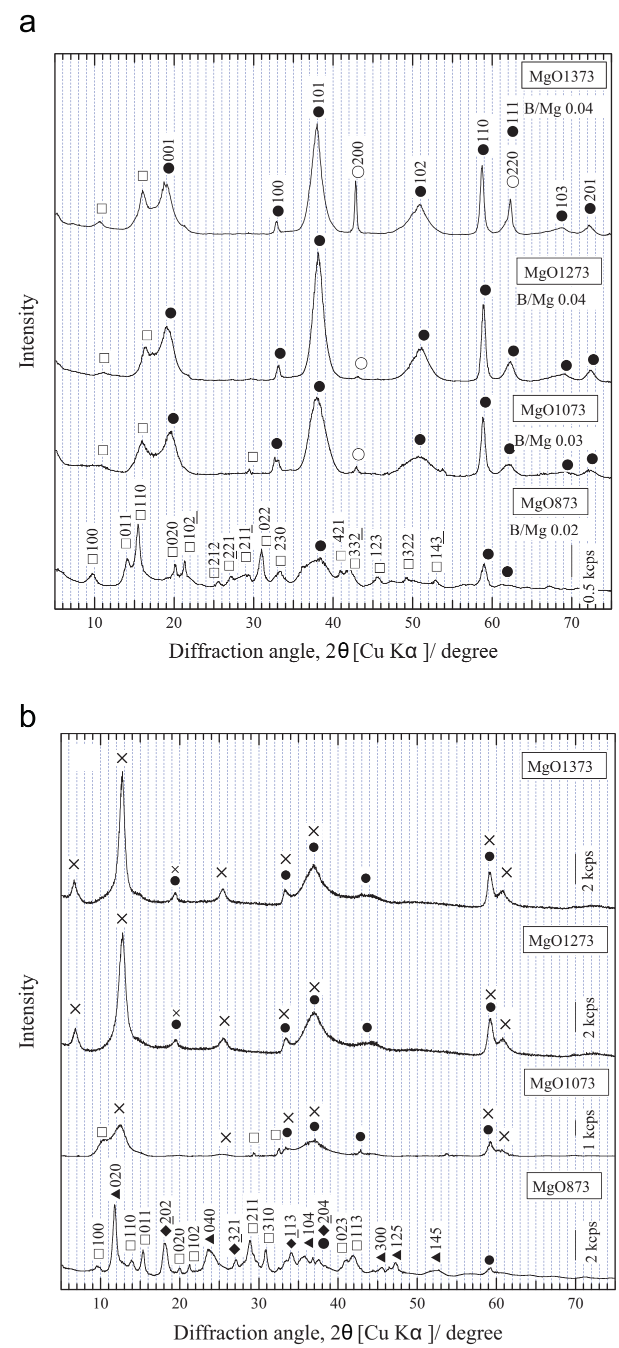

Fig. 7. XRD patterns of solid residues after sorption of (a) 6.08 mM and (b) 67.9 mM B on MgO873, MgO1073, MgO1273, and MgO1373. Symbols: ○, MgO; ●, $Mg(OH)_2$ (JCPDS 44-1482); □, $Mg_5(CO_3)_4(OH)_2 \cdot 4H_2O$ (JCPDS 25-513); ◇, $Mg_7(CO_3)_5(OH)_4 \cdot 24H_2O$ (JCPDS 47-1880); ◆, $MgB_3O_3(OH)_2 \cdot 5H_2O$ (JCPDS 7-595); ×, $Mg_7B_4O_{13} \cdot 7H_2O$ (magnesium borate hydrate) (JCPDS 019-0754).

The newly produced $Mg_5(CO_3)_4(OH)_2 \cdot 4H_2O$ is a solid solution of $MgCO_3$ and $Mg(OH)_2$, and can also be expressed as $4MgCO_3 \cdot Mg(OH)_2 \cdot 4H_2O$. At higher calcination temperatures, the relative intensities of residual MgO were larger, and the $Mg(OH)_2$ formed was more crystalline, but the crystallinity of the $Mg_5(CO_3)_4(OH)_2 \cdot 4H_2O$ that formed was not affected very much (Fig. 7(a)). With MgO873, less crystalline $Mg(OH)_2$ and more crystalline $Mg_5(CO_3)_4(OH)_2 \cdot 4H_2O$ were formed. The basic magnesium carbonates are expected to form by reaction of released Mg^{2+} ions from poorly crystalline magnesium oxide with carbon dioxide derived from air when the pH is not high enough to precipitate $Mg(OH)_2$.

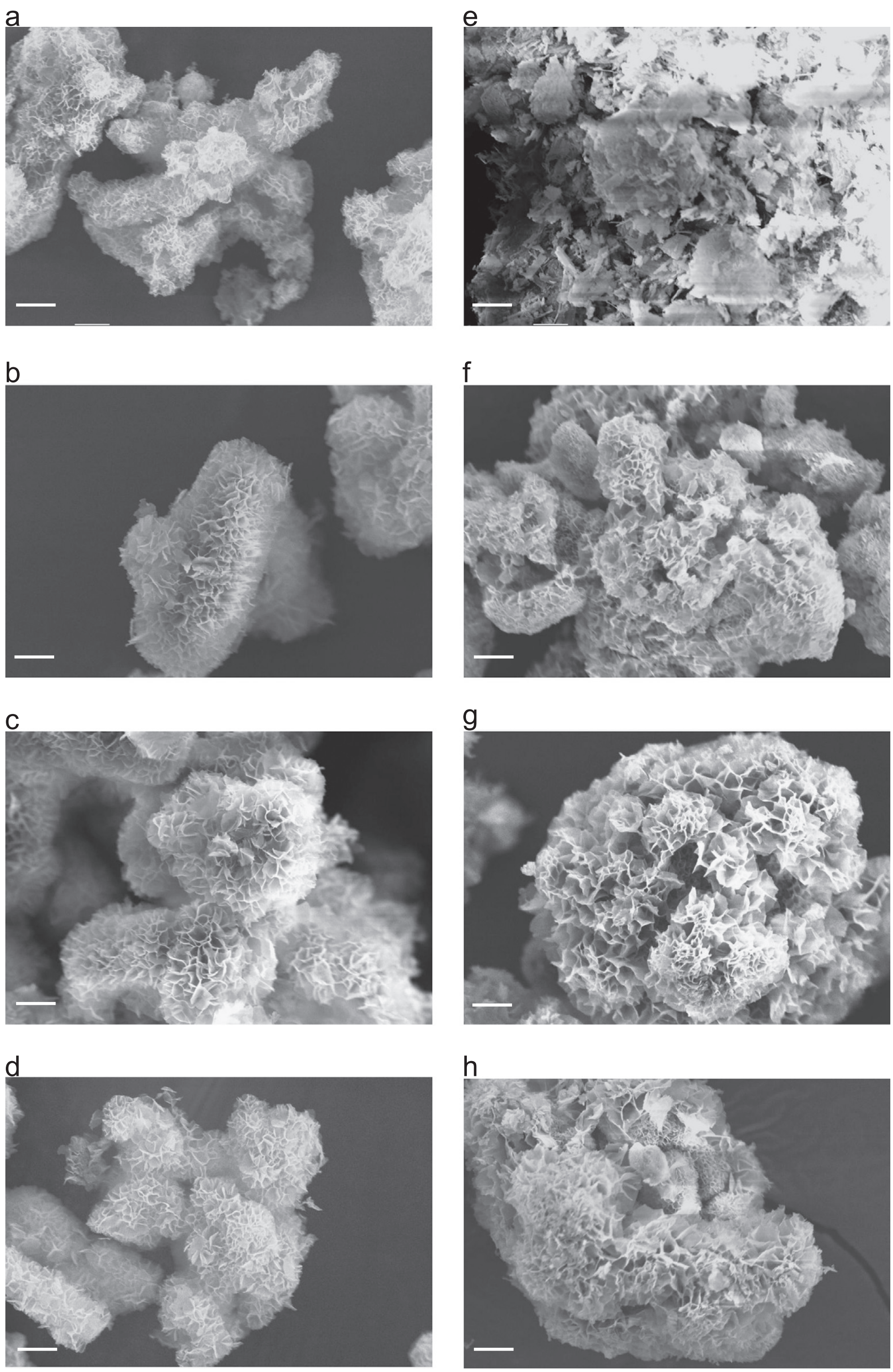

Fig. 8. SEM images of solid residues after sorption of (a)–(d) 6.08 mM and (e)–(h) 67.9 mM boron on: MgO873 ((a), (e)); MgO1073 ((b), (f)); MgO1273 ((c), (g)) and MgO1373 ((d), (h)). The scale bars indicate 5 μm.

The equilibrium pH after sorption of borate is higher for sorbents which were calcined at higher temperatures (Fig. 5(c)); this would facilitate the precipitation of $Mg(OH)_2$. Based on this mechanism for reaction of borate with magnesium oxide, greater basicity was obtained at higher calcination temperatures in Fig. 4. This then meant that ligand-promoted dissolution of MgO was more feasible, and led to more effective immobilization of borate in $Mg(OH)_2$ phase. In contrast, for samples calcined at lower temperatures, the calcined products are less basic, and thus ligand-promoted dissolution of MgO is less feasible. Therefore, the fate of free Mg^{2+} ions derived from simple dissolution of lower crystallinity MgO, is to be precipitated as basic magnesium carbonates, as shown in Fig. 7(a), because the solution becomes super-saturated with respect to $Mg_5(CO_3)_4(OH)_2 \cdot 4H_2O$. This precipitation is expected to contribute negligibly to immobilization of boron, because the magnesium carbonate complex does not involve borate. The boron to magnesium molar ratio in the solid residues ranged from 0.02 to 0.04 (Fig. 7(a)), where the smaller values were obtained with the lower calcination temperatures.

Meanwhile, after sorption of 67.9 mM borate on MgO1073, MgO1273, and MgO1373, peaks assigned to magnesium borate hydrate ($Mg_7B_4O_{13} \cdot 7H_2O$, JCPDS 019-0754) were observed, along with $Mg(OH)_2$, in the solid residues (Fig. 7(b)). The magnesium borate hydrate is not an oxide, but instead is basic magnesium borate triborate, expressed as $Mg_7(OH)_7(B(OH)_4)[B_3O_6(OH)_3]$, which is precipitated through the complex $[MgB(OH)_4]^+$, produced as an intermediate during ligand-promoted dissolution of MgO. For MgO873, kurnakovite ($MgB_3O_3(OH)_5{\cdot}5H_2O$, JCPDS 7-596) was formed, as well as $Mg(OH)_2$ and $Mg_5(CO_3)_4(OH)_2 \cdot 4H_2O$. Kurnakovite is a solid solution of $Mg(OH)_2$ and $B_3O_3(OH)_3$, expressed as $Mg(OH)_2B_3O_3(OH)_3 \cdot 5H_2O$. The boron to magnesium molar ratio in the solid residues, at this higher boron concentration, ranged from 0.24 to 0.43, where the smaller values were obtained for sorbents calcined at lower temperatures. In the presence of high boron concentrations, both precipitation involving boron species and co-precipitation with $Mg(OH)_2$ contribute to tri-dimensional immobilization of B. In Fig. 6(a), precipitation involving boron species is responsible for the increase in gradient of the sorption isotherms when C_e is greater than 30 mM. With the increased initial boron concentration, a lower equilibrium pH was observed; this then interferes with the precipitation of $Mg(OH)_2$. The suppression of magnesium hydroxide precipitation also suggests that H_3BO_3 interferes with the access of water molecules to MgO surfaces. Therefore, magnesium ions, in the presence of high boron concentrations, are incorporated into

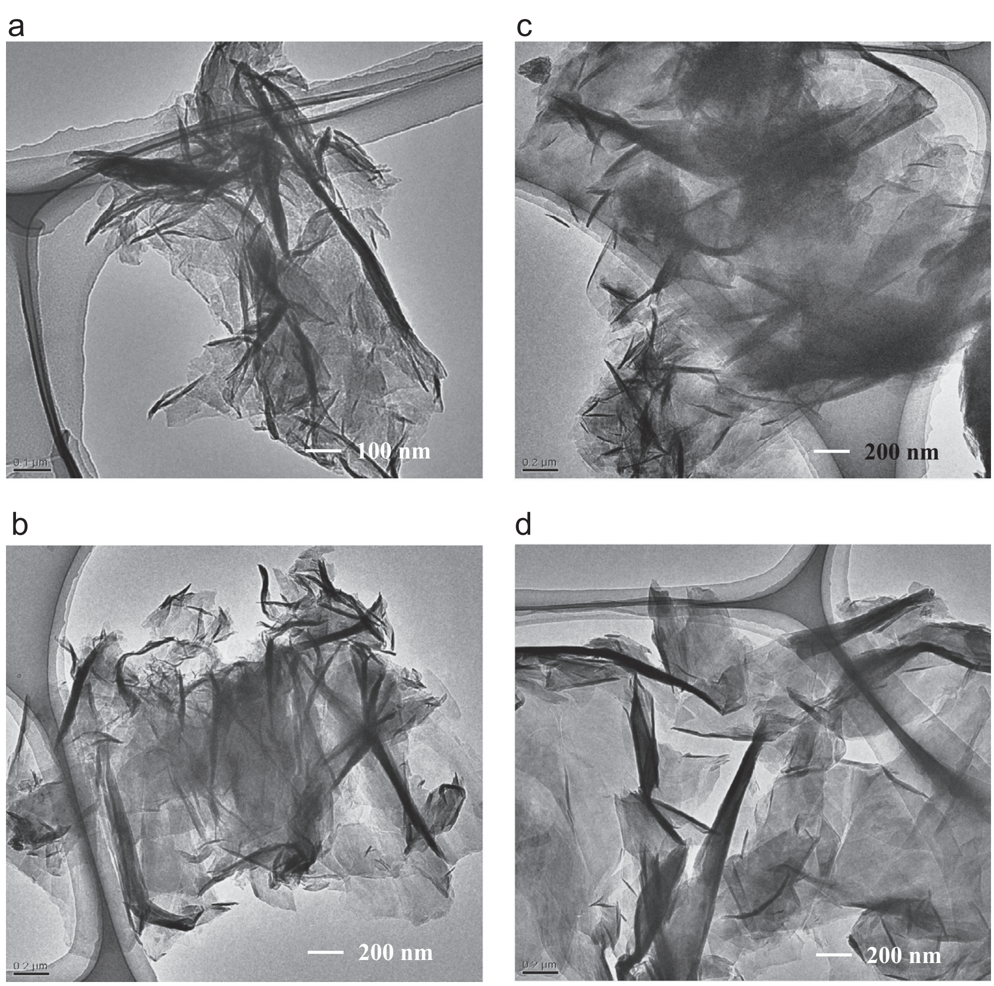

Fig. 9. TEM images of the solid residues after sorption of 6.08 mM boron on (a) MgO873, (b) MgO1073, (c) MgO1273, and (d) MgO1373.

magnesium borate hydrate precipitates; for example, ΔG_f^0 is - 8449.59 kJ/mol for $MgB_3O_3(OH)_5 \cdot 5H_2O$ [32].

SEM images of solid residues after sorption of borate showed that the surface morphologies had clearly changed (Fig. 8). The images of the calcined products were similar, independent of calcination temperature, and showed rod-shaped crystals, 5–6 μm in diameter. After sorption of 6.08 mM borate, the surface morphologies of the solid residues changed into honeycomb structures, probably from partial dissolution of MgO and formation of bulky $Mg(OH)_2$ (Fig. 8 (a)–(d), Fig. S1). In the solid residues after sorption of 67.9 mM borate, segregation of each particle seems to have progressed, and regular honeycomb structure is hard to see (Fig. 8(e)–(h)); this is probably because of the formation of additional $Mg_7B_4O_{13}$ phase (Fig. 7(b)).

TEM images of the solid residues after sorption of 6.08 mM borate were totally different from those before sorption of borate (Fig. 9). As can be seen in the XRD results (Fig. 7(a) and (b)), as boron concentration increases, peaks from *hk*0 planes become narrower, while those from *hkl* planes are broadened. This occurs because immobilized H_3BO_3 interferes with stacking along the *c*-axis direction of $Mg(OH)_2$. According to Fig. 6(b), sorption densities are similar for MgO1073, MgO1273 and MgO1373 at the initial boron concentration of 6.08 mM, and are around double that of MgO873. The TEM images show developed plate-like crystals, consistent with the XRD results shown in Fig. 7(a). The crystal size of the plates in solid residues is affected by the calcination temperature used for the sorbent: the largest plates occur for MgO1273 and MgO1373, whilst much smaller crystals occur for MgO873. It can be seen that sorption of borate did not interfere with the expansion and flaking of the plates in $Mg(OH)_2$.

4. Conclusions

MgO-rich phases were formed by calcination of magnesium carbonate at 873, 1073, 1273 or 1373 K for 1 h. Higher calcination temperatures led to higher crystallinity of MgO, and greater efficiency in removal of borate. The efficiency of removal of borate was reasonably well correlated with the basicity per unit surface area of magnesium oxide in each product, as obtained from CO_2-TPD analysis, and did not depend upon specific surface area. The greater basicity with higher calcination temperature promotes processes in which a molecular form of boric acid accesses the surface of magnesium oxide. The final pH values after sorption of borate always increased, and were sufficient to lead to super saturation with respect to $Mg(OH)_2$. It is considered that the borate removal process can be divided into co-precipitation with $Mg(OH)_2$ and precipitation of $Mg_7B_4O_{13} \cdot 7H_2O$ and $MgB_3O_3(OH)_5 \cdot 5H_2O$. At high borate concentrations, the additional mechanism of precipitation of boron-containing species such as $Mg_7B_4O_{13} \cdot 7H_2O$ and $MgB_3O_3(OH)_5 \cdot 5H_2O$ contributes to immobilization of boron. In this concentration range, the sorption isotherms do not show Freundlich behavior—instead the gradient of the sorption density curve increases with increasing concentration. Calcination temperatures directly affect the efficiency of decarbonation of magnesium carbonate and the basicity of the magnesium oxide contained within the calcined products; these factors, as well as boron concentration, significantly influence the immobilization mechanism of borate on the calcined MgO-rich phases.

Acknowledgment

Financial support was provided to KS by JSPS Funding Program for Next-Generation World Leading Researchers (NEXT Program) GR078. TEM observation was conducted in high voltage electron microscopy (HVEM), Kyushu University.

Appendix A. Supporting information

Supplementary data associated with this article can be found in the online version at http://dx.doi.org/10.1016/j.ceramint.2013.07.056.

References

[1] T. Sutton, U. Baumann, J. Hayes, N.C. Collins, B.-J. Shi, T. Schnurb, A. Hay, G. Mayo, M. Pallotta, M. Tester, P. Langridge, Boron-toxicity tolerance in barley arising from efflux transporter amplification, Science 318 (5855) (2007) 1446–1449.

[2] R. Liu, J. Wilmalasea, R.L. Bowen, C.S. Atwood, Luteining hormone receptor mediates neuronal pregnenolone production via up-regulation of steroidogenic acute regulatory protein expression, Journal of Neurochemistry 100 (2007) 1329–1339.

[3] U. Sayli, Y. Tekdemysr, H.E. Cubuk, S. Avci, E. Tüccar, H.A. Elhan, A. Uz, The course of the special peroneal nerve: an anatomical cadaver study, Foot and Ankle Surgery 4 (1998) 69 (69).

[4] WHO, Environmental Health Criteria Monograph, IPCS, Geneva204.

[5] R.O. Nable, G.S. Banuelos, J.G. Paul, Boron toxicity, Plant and Soil 193 (1997) 181–198.

[6] D.W. Blowes, C.J. Ptacek, S.G. Bernner, C.W.T. Mcrae, R.W. Puls, Treatment of dissolved metals and nutrients using permeable reactive barriers, Journal of Contaminant Hydrology 45 (2000) 123–137.

[7] M.M. Scherer, S. Richter, R.L. Valentine, P.J.J. Alvarez, Chemistry and microbiology of permeable reactive barriers for in situ groundwater clean up, Environmental Science and Technology 30 (2000) 363–411.

[8] D.L. Naftz, S.J. Morrison, C.C. Fuller, J.A. Davis, Handbook of Groundwater Remediation Using Permeable Reactive Barriers: Applications to Adionuclides, Trace Metals, and Nutrients, Academic Press, San Diego, CA, 2003.

[9] J. Wolska, M. Bryjak, Methods for boron removal from aqueous solutions—a review, Desalination 310 (2013) 18–24.

[10] Z.C. Celik, B.Z. Can, M.M. Kocakerim, Boron removal from aqueous solutions byactivatedcarbon impregnated with salicylic acid, Journal of Hazardous Materials 152 (2008) 415–422.

[11] W. Bouguerra, A. Mnif, B. Hamrouni, M. Dhahbi, Boron removal by adsorption onto activated alumina and by reverse osmosis, Desalination 223 (2008) 31–37.

[12] S. Karahan, M. Yurdako, Y. Seki, K. Yurdako, Removal of boron from aqueous solution by clays and modified clays, Journal of Colloid and Interface Science 293 (2006) 36–42.

[13] R. Keren, F.T. Bingham, Boron in water, soils, and plants, Advances in Soil Sciences 1 (1985) 229–276.

[14] S. Goldberg, H.S. Froster, S.M. Lesch, E.L. Heick, Influence of anion competition on boron adsorption by clays and soils, Soil Science 161 (1996) 99–103.

[15] N. Öztürk, D. Kavak, Adsorption of boron from aqueous solutions using fly ash: Batch and column studies, Journal of Hazardous Materials 127 (2005) 81–88.

[16] M.M. De La Fuente García-Soto, E.M. Camacho, Boron removal by means of adsorption with magnesium oxide, Separation and Purification Technology 48 (2006) 36–44.

[17] K. Sasaki, N. Fukumoto, S. Moriyama, T. Hirajima, Sorption characteristics of fluoride on to magnesium oxide-rich phases calcined at different temperature, Journal of Hazardous Materials 191 (2011) 240–248.

[18] R.Y. Zhang, J.G. Lion, Significance of magnesite paragenesis in ultrahigh-pressure metamorphic rocks, American Mineralogist 79 (1994) 397–400.

[19] M.A. García, J.M. Chimenos, A.I. Fernández, L. Miralles, M. Segarra, F. Espiell, Low-grade MgO used to stabilize heavy metals in highly contaminated soils, Chemosphere 56 (2004) 481–491.

[20] S. Zhang, F. Cheng, Z. Tao, F. Gao, J. Chen, Removal of nickel ions from wastewater by $Mg(OH)_2$/MgO nanostructures embedded in Al_2O_3 membranes, Journal of Alloys and Compounds 426 (2006) 281–285.

[21] V.S.S. Birchal, S.D.F. Rocha, V.S.T. Ciminelli, The effect of magnesite calcination conditions on magnesia hydration, Minerals Engineering 13 (2000) 1629–1633.

[22] K. Sasaki, X. Qiu, S. Moriyama, C. Tokoro, K. Ideta, J. Miyawaki, Characteristic sorption of $H_3BO_3/B(OH)_4^-$ on magnesium oxide. Materials Transactions, http://dx.doi.org10.2320/matertrans.M-M2013814, in press.

[23] L.F. Amaral, I.R. Oliveira, P. Bonadia, R. Salomão, V.C. Pandolfelli, Chelants to inhibit magnesia (MgO) hydration, Ceramics International 37 (2011) 1537–1542.

[24] N.C. Halder, N.C.J. Wagner, Separation of particle size and lattice strain in integral breadth measurements, Acta Crystallographica 20 (1966) 312–313.

[25] A. Korchef, Y. Champion, N. Njah, X-ray diffraction analysis of aluminum containing Al_8Fe_2Si processed by equal channel angular pressing, Journal od Alloys and Compounds 427 (2007) 176–182.

[26] Y. Sawada, J. Yamaguchi, O. Sakurai, K. Uematsu, N. Mizutani, M. Kato, Thermogravimetric study on the decomposition of hydromagnesite 4 $MgCO_3 \cdot Mg(OH)_2 \cdot 4\ H_2O$, Thermochimica Acta 33 (1979) 127–140.

[27] C.E. Sjögren, C. Johansson, A. Nævestad, K. Briley-Sæbø, A.K. Fahlvik, Crystal size and properties of superparamagnetic iron oxide (SPIO) particles, Magnetic Resonance Imaging 15 (1997) 55–67.

[28] M.S. Mel'gunov, V.B. Fenelonov, E.A. Mel'gunova, A.F. Bedilo, K.J. Klabunde, Textural changes during topochemical decomposition of nanocrystalline Mg(OH)2 to MgO, Journal of Physical Chemistry B 107 (2003) 2427–2434.

[29] H.N. Ramesh, S.D. Venkataraja Mohan, Compaction characteristics of alkalis treated expansive and non-expansive soil contaminated with acids, in: Proceedings of the Indian Geotechnical Conference, Kochi, India, 2011, pp. 733–736.

[30] R.L. Bassett, A critical evaluation of the thermodynamic data for boron ions, ion pairs, complexes, and polyanions in aqueous solution at 298.15 K and 1 bar, Geochimica Cosmochimica Acta 44 (1980) 1151–1160.

[31] J.L. Anchel, A.C. Hess, H_2O dissociation at low-coordinated sites on $(MgO)n$ Clusters, $n=4$, 8, Journal of Physical Chemistry 100 (1966) 18317–18321.

[32] J. Li, B. Li, S. Gao, Calculation of thermodynamic properties of hydrated borates by group contribution method, Physics and Chemistry of Minerals 27 (2000) 342–346.